Chemical Papers (2022) 76:4245–4260
https://doi.org/10.1007/s11696-022-02179-z

ORIGINAL PAPER

Catalytic performance improvement with metal ion changes for efficient, stable, and reusable superoxide dismutase–metalphosphates hybrid nanoflowers

Burcu Somtürk Yılmaz[1] · Serkan Dayan[2] · Nalan Özdemir[1] · Nilgün Kalaycioğlu Özpozan[1]

Received: 18 October 2021 / Accepted: 15 March 2022 / Published online: 29 March 2022

Abstract

Herein, for the first time, the flower-like enzyme–inorganic hybrid nanoflowers were synthesized using a superoxide dismutase (SOD) as organic material and selected some metal ions (Cu(II), Co(II), Mn(II) and Zn(II)) as inorganic parts at optimum pH value. The synthesis steps of SOD@metalphosphates hybrid nanoflowers were verified by XRD, FT-IR, FESEM, and EDX. The synthesized nanoflowers were utilized as a catalyst in the reduction of organic pollutants (2-nitrophenol (2-NP) and Rhodamine *B* (RhB)) with $NaBH_4$ in aqueous media for catalytic properties and susceptibility. The activities of both the substrate and the metal center of the catalyst were determined in the increasing rate order of RhB > 2-NP for substrate and $SOD@Cu_3(PO_4)_2{\cdot}3H_2O > SOD@Co_3(PO_4)_2{\cdot}8H_2O > SOD@Mn_3(PO_4)_2{\cdot}7H_2O > SOD@Zn_3(PO_4)_2{\cdot}4H_2O$ hNfs for catalysts. The catalytic data provided herein by using SOD@metalphosphates ($SOD@Cu_3(PO_4)_2{\cdot}3H_2O$, $SOD@Co_3(PO_4)_2{\cdot}8H_2O$, $SOD@Mn_3(PO_4)_2{\cdot}7H_2O$ and $SOD@Zn_3(PO_4)_2{\cdot}4H_2O$) nanoflowers suggest that the materials can be effective catalysts for the water-based reduction reaction of organic pollutants.

✉ Nalan Özdemir
ozdemirn@erciyes.edu.tr

[1] Department of Chemistry, Faculty of Science, Erciyes University, 38039 Kayseri, Turkey

[2] Drug Application and Research Center, Erciyes University, 38280 Kayseri, Turkey

Graphical abstract

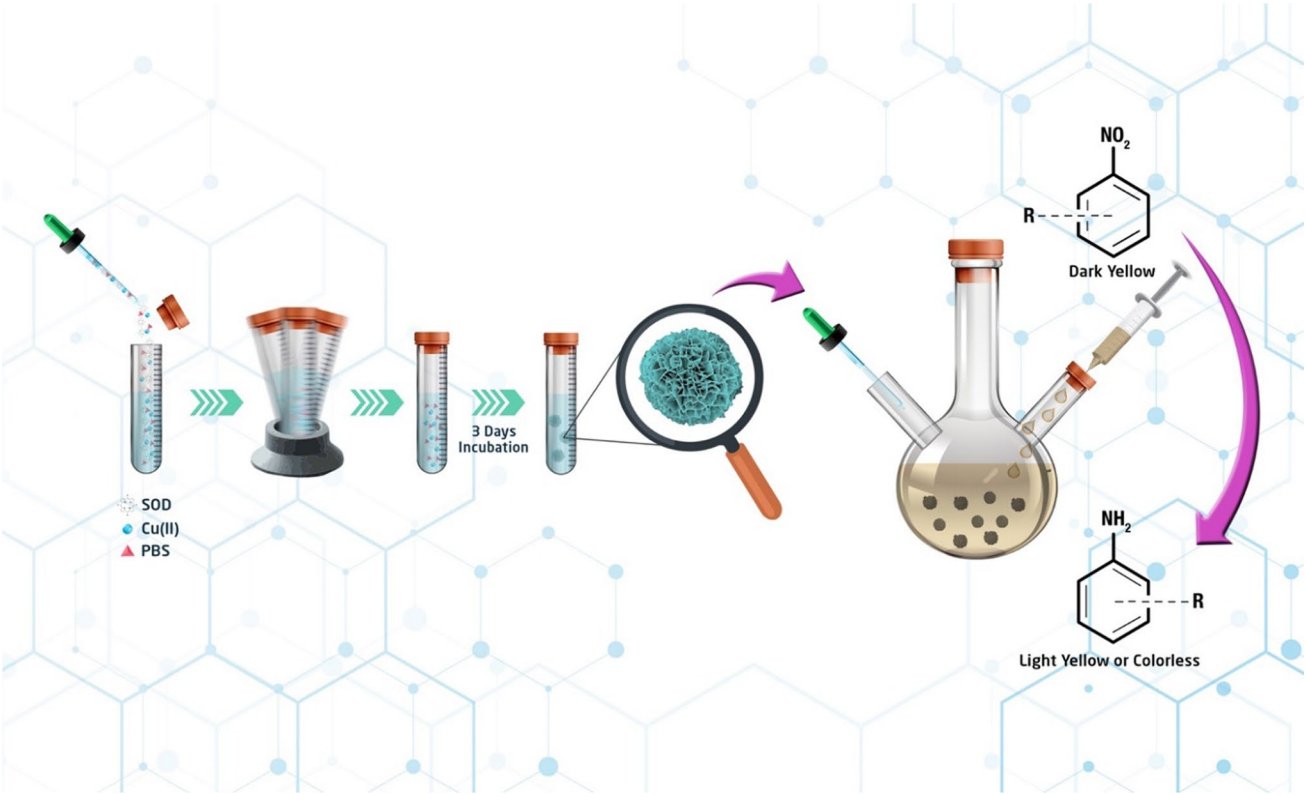

Keywords Hybrid nanoflowers · Superoxide dismutase · Reduction of organic pollutants · Catalysts

Introduction

Enzymes are proteins that catalyze reactions at very high speeds (Erdem et al. 2015; Arsalan et al. 2020). It is an alternative to chemical catalysts with its features such as high catalytic efficiency and selectivity, low toxicity and water solubility and is widely used in fields such as biochemistry, biomedical, food and chemistry. Enzymes have been recognized remarkably as biocatalysts in various industries due to their green chemistry and substrate specificity. However, free (soluble) forms of enzymes have a short lifetime, and therefore soluble enzymes cannot be exploited on a large scale, limiting their application in many areas and also, the separation of the soluble enzyme from the reaction medium is difficult which makes it impossible to reuse (Madhu and Chakraborty 2017; Zhao et al. 2019). To be used in practice, it is necessary to increase the efficiency, activity, stability, and recovery of enzymes, especially as industrial biocatalysts. To increase the use of enzymes as industrial biocatalysts, stable preparations of enzymes with improved operational stability need to be obtained. Immobilization is one of the important ways enzymes stabilize. Many immobilization methods have been described and used in the literature to overcome possible problems on stability problems of enzymes and to optimize various applications. There are five different approaches in covalent binding, cross-linking, adsorption, arrest, and encapsulation in enzyme immobilization (Wells and Meyer 2014; Shcharbin et al. 2019; Mohamed et al. 2013; Kim et al. 2006). However, in immobilization studies, except for a few enzymes, the activity of the immobilized enzymes increased compared to the free enzyme, but their activity decreased (Sassolas et al. 2012; Netto et al. 2013; Wei et al. 2008). But, first, a new and different immobilized enzyme application with increased efficacy was suggested by Zare et al. (Ge et al. 2012).

Zare et al. reported the formation method of flower-like protein–inorganic hybrid nanoflowers using Cu (II) ion as inorganic components, they are called as "nanoflowers" in the literature, and various proteins and enzymes (lactalbumin, laccase, carbonic anhydrase, lipase, and BSA) as an organic component. In the past few years, the synthesis of enzyme–inorganic hybrid nanostructures has been carried out including pancreatin (a mixture of a-amylase, lipase and

protease) (Aydemir et al. 2020), lipase(Wu et al. 2014; Lin, et al. 2014a, b; Lee et al. 2017; Altinkaynak et al. 2020), glucose oxidase (GOD) (Sun et al. 2014), α-amylase(Wang et al. 2013), urease (Somturk et al. 2016), trypsin (Lin, et al. 2014a, b), chymotrypsin (Yin et al. 2015), papain (Liang et al. 2015), laccase (Fu et al. 2019), glucoamylase (Nadar et al. 2016), NADH oxidase (Patel et al. 2017), Cytochrome P450 (He et al. 2017), lactoperoxidase (Altinkaynak et al. 2016), L-asparaginase (Noma et al. 2020), etc.

In principle, the formation of flower-like enzyme–inorganic hybrid nanostructures takes place in three stages: in the first stage, primary metalphosphate crystals are formed depending on the type of metal. Through the coordination of amino groups in the structure of enzymes with metal ions, complexes are formed. In the second stage of growth, large aggregates of biomolecules and primary crystals are formed, flower-like petals appear. In the last step, anisotropic growth causes the formation of a branched flower-like structure. For this reason, the synthesized structures were named "Flower-shaped Hybrid Nanostructures" (Flower-Like Hybrid nanostructures).

Superoxide dismutase (Superoxide Oxidoreductase, E.C: 1.15.1.1, SOD) is a metalloenzyme that catalyzes the dismutation of superoxide anion radicals into molecular oxygen and hydrogen peroxide. This enzyme was detected in oxygen-breathing organisms in 1968 and catalyzes the conversion of superoxide to hydrogen peroxide and molecular oxygen. Hydrogen peroxide is then inactivated by the enzyme glutathione peroxidase and catalase. It plays an important role in controlling superoxide levels in cell divisions (Durak et al. 1996). SOD is found in all cells that metabolize oxygen. It is an important defense against oxygen toxicity (Weselake et al. 1986). The use of SOD as a catalyst and its activity in enzymatic reactions have highlighted its use as a ligand in catalyst chemistry. Herein, SOD@metallophosphate structures with both increased surface area and ligand effect were tested together with metallophosphate structures.

Although the nitro compounds from organic-based paints are used in many industrial applications they are known as important environmental pollutants, and the degradation of these pollutants has recently been preferred. The amino compounds produced as a result of this degradation process are the compounds used in the production of qualified chemicals (Sargin, Baran, and Arslan 2020; Moradi et al. 2020; Xu et al. 2020; Denizalti et al. 2020), which are listed as chelating agents, fibers/nanofibers, agricultural drugs, cosmetics, polymer fabrication, dye-based materials, pharmaceuticals, etc. (Du et al. 2020; Dell'Anna et al. 2014; Das et al. 2019). Also, the studies are carried out to obtain the most ideal catalyst and catalytic conditions in degradation studies and both easily producible and production of high-performance catalysts become important. Recent times, the various metals (copper (Dayan, Altinkaynak, et al. 2020), cobalt (Sheng et al. 2020), palladium (Dayan, et al. 2020a, b, c; Zhang et al. 2020), ruthenium,(Jia, Wang, and Zhi 2020; Liew et al. 2017) silver (Bahadorikhalili et al. 2020; Ansari et al. 2019), nickel (Advani et al. 2020), etc.) as catalysts were tested in the reduction/degradation reactions. The performances of different metals in catalytic reactions are also quite different from each other and high-performance works with low-cost metals are also preferred. The catalytic studies of organic–inorganic hybrid nanoflowers have attracted attention in recent years (Ahmadpoor et al. 2021; Dayan, Altinkaynak, et al. 2020; Alhayali et al. 2021) and the nanoflowers with the obtained organic molecules from plant sources using separation purification processes were fabricated and their catalytic properties were examined (Ahmadpoor et al. 2021).

Herein, for the first time, the flower-like enzyme–inorganic hybrid nanoflowers were synthesized using a superoxide dismutase (SOD) as an organic part and some divalent metal ions (Cu(II), Co(II), Mn(II), and Zn(II)) as inorganic parts at optimum pH value. The fabricated SOD@metalphosphates hybrid nanoflowers as catalysts were used in the degradation of organic pollutants (2-nitrophenol and Rhodamine B). It was determined that the difference of the metal center directly affects the catalytic activity. It is predicted that the catalytic activity may also change with different metals. This is expected and compatible with the Irving-Williams series. Although it is not a surprise, the catalytic activities of nanoflowers with different metals are detailed in this work and this is among the first in the literature.

Experimental

Materials

Superoxide dismutase, albumin from bovine serum (BSA) (lyophilized powder), copper sulfate pentahydrate ($CuSO_4{\cdot}5H_2O$) and zinc acetate dihydrate ($Zn(CH_3COO)_2{\cdot}2H_2O$) were purchased from Sigma-Aldrich (USA). Salts (NaCl, KCl, KH_2PO_4, Na_2HPO_4, $CaCl_2{\cdot}2H_2O$, and $MgCl_2{\cdot}6H_2O$) were also obtained from Sigma-Aldrich and utilized for the synthesis of the pH solutions. Cobalt(II) sulfate heptahydrate ($CoSO_4{\cdot}6H_2O$) was obtained from across organics and manganese(II) sulfate monohydrate ($MnSO_4{\cdot}H_2O$) was obtained from bioshop. Ultrapure water was used to prepare aqueous solutions throughout the work.

Synthesis of SOD@metalphosphates hybrid nanoflowers

SOD@metalphosphates hybrid nanoflowers (SOD@metalphosphates hNfs) were prepared according to two different methods depending on the type of metal ion (Cu(II), Co(II),

Mn(II) and Zn(II)) (Gao et al. 2020; Somturk et al. 2016). In the first method (for Cu(II) and Mn(II) ions), $CuSO_4{\cdot}5H_2O$ and $MnSO_4{\cdot}H_2O$ (120 mM) solutions were prepared using purified water. A certain volume of this solution was then added to 10 mM PBS (phosphate-buffered saline) solution (pH 7.4), including 0.02 mg mL^{-1} SOD. The mixture was vortexed vigorously for 30 s and incubated without disturbing for 3 days at + 4 °C (Fig. 1 (a)). After incubation period, to obtain precipitates, each reaction tube was centrifuged at 10.000 rpm for 15 min. Finally, the collected SOD@metalphosphates hNFs were dried at room temperature.

In the second method (for Co(II) and Zn(II) ions), SOD@metalphosphates hNfs were synthesized based on a method determined by Zhang et al. and making some modifications (Zhang et al. 2016; Kim et al. 2016). For this purpose, $Zn(CH_3COO)_2{\cdot}2H_2O$ and $Co(NO_3)_2{\cdot}6H_2O$ (0.05 g/L) solutions were prepared. After that, 16 mg SOD and a certain volume of metal ion solution were added into 20 mL phosphate buffer saline solution (pH 7.4). The mixtures were left on the magnetic stirrer for 24 h at room temperature. After incubation, they were centrifuged at 10.000 rpm for 15 min. Finally, the collected SOD@inorganic hybrid nanoflowers were dried at room temperature (Fig. 1 (b)).

Characterization of SOD@metalphosphates hNfs

The surface morphologies of the fabricated SOD@metalphosphates hNfs were recorded by using field emission scanning electron microscope (FESEM, Zeiss GeminiSEM 500). The elemental weight and atomic percentage analyses of Cu,

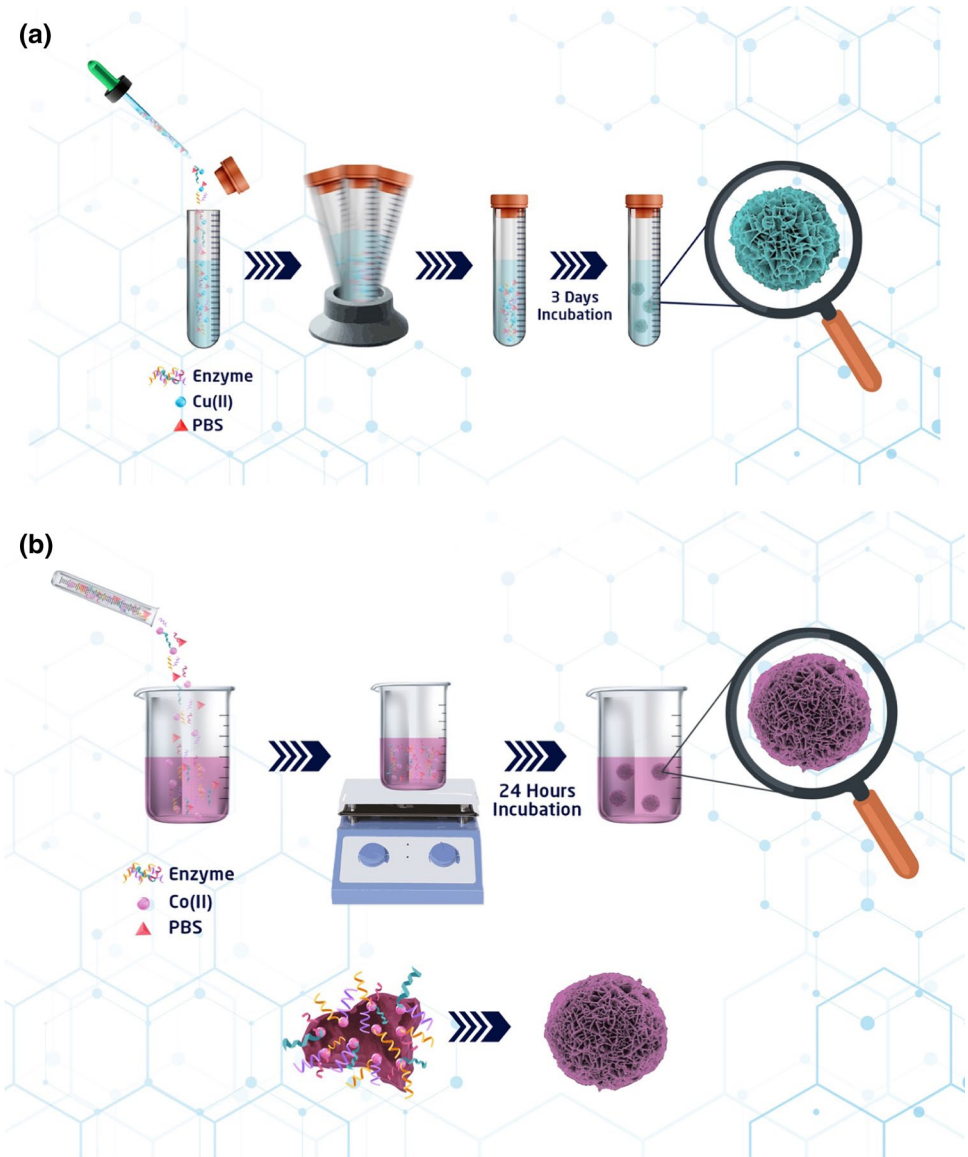

Fig. 1 Representative fabrication scheme of **a** SOD@$Cu_3(PO_4)_2{\cdot}3H_2O$·hNfs and **b** SOD@·$Co_3(PO_4)_2{\cdot}8H_2O$·hNfs

Co, Zn, and Mn elements (also other elements such as *N*, *P*, and *O* from the organic materials (SOD) and phosphate group) in SOD@metalphosphates hNFs were separately assigned by the energy-dispersive *X*-ray (EDX) technique. The chemical-crystal structure of SOD@metalphosphates hNfs was analyzed by using *X*-ray diffraction (Malvern Panalytical XRD) and Fourier transform infrared spectroscopy (FT-IR) (PerkinElmer Spectrum 400). Size analysis of hybrid nanostructures was determined using the Image ProPlas 6.0 program. At the same time, the protein content of SOD@metalphosphates hNfs was determined using Bradford method (Somturk et al. 2016). The encapsulation rate was determined for the synthesized SOD@metalphosphates hNfs. The encapsulation rates were determined to vary between 87 and 95%.

The testing of SOD@metalphosphates hNfs as a catalyst

The catalytic activities of SOD@metalphosphates hNfs were evaluated in the reduction of 2-nitrophenol (2-NP) and Rhodamine B (RhB) using $NaBH_4$ ion as a hydrogen source at ambient temperature with an aqueous solution.

In a typical reaction, a 1.0 mg of the SOD@metalphosphates hNfs was first prepared and added to the solution of nitrophenols or dyes and $NaBH_4$ (0.03 M, freshly, optimum concentration (Dayan, Altinkaynak, et al. 2020; Dayan, Kayaci, Dayan, et al. 2020a, b, c; Dayan et al. 2015a, b; Dayan et al. 2015a, b) in deionized water (10 mL) at ambient temperature and stirred in a clean tube. After the desired time, the reaction samples of the catalytic mixture as a small amount were taken out of the tube and filtered through the micro-column with cotton for the measurement of the absorbance spectra. The catalytic efficiencies of the SOD@metalphosphates hNfs catalysts were seen by comparing the bands which appeared and disappeared after reduction on the UV–Vis spectrum.

Results and discussion

The specific surface morphologies of the fabricated SOD@metalphosphates hNfs in pH 7.4 at room temperature were evaluated by FESEM analysis and the images were confirmed to be flower-like (known as nanoflowers). Average nanoflower dimensions for the SOD@$Cu_3(PO_4)_2{\cdot}3H_2O$·hNfs, SOD@$Co_3(PO_4)_2{\cdot}8H_2O$ hNfs, SOD@$Mn_3(PO_4)_2{\cdot}7H_2O$ hNfs and SOD@$Zn_3(PO_4)_2{\cdot}4H_2O$ hNfs were recorded as ~ 7.11 µm, ~ 8.97 µm, ~ 10.29 µm, ~ 2.23 µm, respectively (Fig. 2). As seen in Fig. 2, as the metal content changes, there are obvious differences in FESEM images. Also, all the materials were recorded to be in a sphere type formation and FESEM images were reported as a visual counterpart of the effect of metal centers on physico-chemical parameters. Herein, the metal (II) ions with the phosphate source form metallophosphates and a specific crystallization occurs during this formation. Especially in the presence of ligand (enzyme or organic molecules), these morphologies differentiate further and the materials are known as nanoflowers. These morphologies depend on the metal ion and ligand, and a coordination bond is formed between metal ions and groups such as *N*, *S* and *O* on ligands and increases the stability of the material.

The elemental composition of the SOD@metalphosphates hNfs was analyzed by the energy-dispersive *X*-ray (EDX) technique (Fig. 3). The founded elements are suitable to $Cu_3(PO_4)_2{\cdot}3H_2O$, $Co_3(PO_4)_2{\cdot}8H_2O$, $Zn_3(PO_4)_2{\cdot}4H_2O$, $Mn_3(PO_4)_2{\cdot}7H_2O$ nanocrystal structures (Cu, Co, Zn, Mn, O, and *P*) and the superoxide dismutase (SOD) (C and N). These EDX peaks were confirmed the formation of the SOD@metalphosphates hNfs structures and the EDX spectrum demonstrated that the average weight and atomic percentages of copper for SOD@$Cu_3(PO_4)_2{\cdot}3H_2O$ hNfs, cobalt for SOD@$Co_3(PO_4)_2{\cdot}8H_2O$ hNfs, zinc for SOD@$Zn_3(PO_4)_2{\cdot}4H_2O$ hNfs, manganese for SOD@$Mn_3(PO_4)_2{\cdot}7H_2O$ hNfs were recorded as 21.7% and 6.7%, 36.5% and 15.3%, 29.4% and 9.0%, 31.8%, and 14.6%, respectively.

Also, the elemental mapping of SOD@metalphosphates hNfs was performed (Fig. 4) and it can be considered as one of the strongest pieces of evidence for the formation of SOD@metalphosphates hNfs. As seen in Fig. 5, the elemental mapping analyses confirm the Cu, Co, Zn, Mn, N, O, and P elements, and the elements are homogeneously distributed inside the SOD@metalphosphates hNfs.

The chemical structure and formation of SOD@metalphosphates hNfs were investigated using the FT-IR (Perkin Elmer Spectrum 400) spectrum. The FT-IR spectrum revealed characteristic peaks of SOD@metalphosphates hNfs (Fig. 5). The data of spectrums of free SOD and SOD@metalphosphates hNfs nanoflowers were seen as follows; *For free SOD, FT-IR* (cm^{-1}): 3270 (N–H and O–H stretching), 3074 (Ar–H, stretching), 2962 (C–H, stretching), 2933 (C–H, stretching), 2872 (C–H, stretching), 1633, 1515, 1449, 1392, 1339, 1309, 1286, 1229, 1159, 1101, 1052, 1026, 931, 821, 736, 695, 665, 642, 623, 604, 575, 543, 525, 488, 470. *For* SOD@$Cu_3(PO_4)_2.3H_2O$ hNfs, *FT-IR* (cm^{-1}): 3303 (N–H and O–H stretching), 2979 (Ar–H and C–H stretching), 2900 (C–H, stretching), 1622, 1541, 1410, 1150, 1041 (P=O), 986, 956 (P–O), 799, 617 (O=P=O), 591, 556 (O=P=O), 504, 492, 483, 475, 467. *For* SOD@·$Co_3(PO_4)_2{\cdot}8H_2O$ hNfs, *FT-IR* (cm^{-1}): 3444 (N–H and O–H stretching), 3191 (Ar–H, stretching), 3046 (C–H, stretching), 1646, 1549, 1396, 1339, 1031 (P=O), 970 (P–O), 937, 832, 694 (O=P=O), 667, 615, 567, 536 (O=P=O), 504, 496, 491, 473, 466, 456. *For*

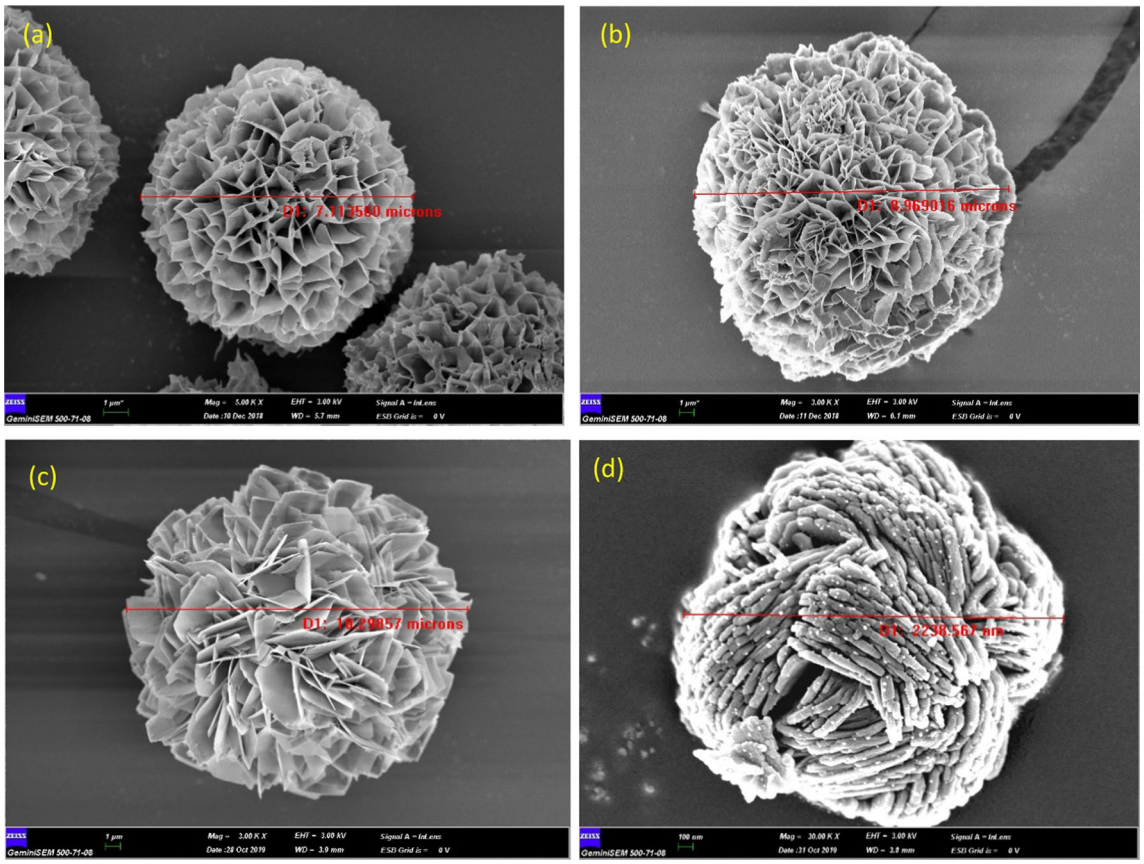

Fig. 2 SEM images of SOD@metalphosphates hNfs using different metal ions: **a** Cu(II), **b** Co(II), **c** Mn(II) and **d** Zn(II)

SOD@$Zn_3(PO_4)_2.4H_2O$ hNfs, *FT-IR* (cm^{-1}): 3531 (N–H and O–H stretching), 3270 (Ar–H, stretching), 3184 (Ar–H, stretching), 2964 (C–H, stretching), 2925 (C–H, stretching), 1645, 1534, 1449, 1402, 1244, 1102, 1065, 1020 (P=O), 999 (P=O), 931 (P–O), 708, 672, 628 (O=P=O), 595, 585, 563 (O=P=O), 535, 519, 507, 497, 489, 480, 473, 455. *For* SOD@$Mn_3(PO_4)_2.7H_2O$ hNfs, *FT-IR* (cm^{-1}): 3600–3200 (N–H and O–H stretching), 3193 (Ar–H, stretching), 2967 (C–H, stretching), 2921 (C–H, stretching), 1634, 1535, 1447, 1404, 1318, 1247, 978 (P=O), 948 (P–O), 810, 752, 689, 666, 542 (O=P=O), 495, 473, 453. The presence of metallophosphate structures can be easily detected in hybrid nanoflowers with the formation of phosphorus and oxygen bonds. The bending vibrations of O=P=O groups in SOD@metalphosphates hNfs were recorded at ~ 551 cm^{-1} and ~ 599 cm^{-1}. The P=O and P–O tension bands appeared at ~ 1042 cm^{-1} and ~ 954 cm^{-1}. The detection of phosphorus–oxygen bonds indicates the formation of metallophosphates, and the frequency shift in the vibrations of these bonds is an indication of the bonding of different metals. It is also a critical indicator for the characterization of a newly formed bond structure relative to the free SOD. Also, the presence of peaks belonging to functional groups originating from SOD in hybrid nanomaterial structures is another confirmation part of the structure. The vibration bands of typical SOD at 1400–1633 cm^{-1} are bound to the NH_2, C=C and C=N groups, and the tensile bands at 2800–3000 cm^{-1} are bound to the $–CH_2$ and $–CH_3$ groups.

The powder *X*-ray diffraction data of the synthesized SOD@metalphosphates hNfs were carried out to determine the crystal structure of nanomaterials (Fig. 6). The XRD peaks were assigned as f*or SOD@*$Cu_3(PO_4)_2{\cdot}3H_2O$ hNfs, *XRD*: 9.10°, 12.96°, 18.79°, 20.87°, 27.38°, 29.48°, 30.64°, 31.74°, 33.71°, 37.21°, 41.59°, 45.48°, 47.74°, 53.46°, 56.48°, 61.10°, 63.57°, 66.22°, 68.19°, 71.42°, 75.26°, 79.06°, 83.95° in Fig. 6(a) compared with JCPDS (00 – 022 – 0548), and for *SOD@*$Co_3(PO_4)_2{\cdot}8H_2O$ hNfs, XRD: 11.29°, 13.34°, 18.38°, 19.66°, 22.05°, 23.26°, 28.02°, 30.35°, 31.74°, 33.24°, 35.81°, 37.42°, 39.16°, 41.59°, 43.85°, 45.53°, 47.37°, 51.83°, 55.27°, 58.87°, 61.50°, 63.15°, 66.22°, 70.69°, 77.62° in Fig. 6(b) compared with JCPDS (00 – 041 – 0375) and for *SOD@*$Zn_3(PO_4)_2{\cdot}4H_2O$ *hNfs*, XRD: 9.68°, 16.83°, 17.54°, 18.35°, 19.45°, 20.21°, 22.21°, 22.99°, 24.55°, 25.83°, 26.36°, 27.46°, 28.67°, 31.48°, 33.95°, 34.45°, 35.79°, 37.18°, 38.49°, 39.73°, 41.20°, 41.99°, 43.12°, 45.47°, 46.92°, 50.07°, 52.99°,

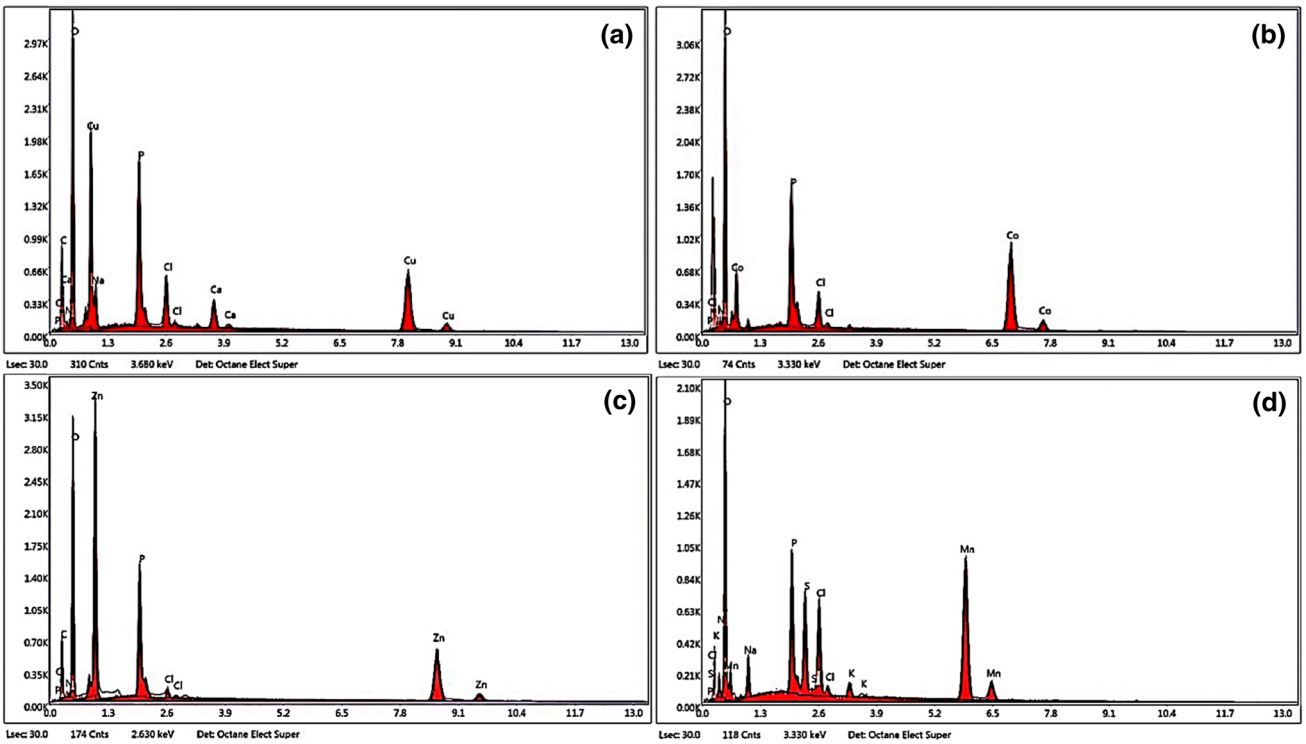

Fig. 3 EDX analysis of SOD@metalphosphates hNfs: **a** SOD@$Cu_3(PO_4)_2{\cdot}3H_2O$·hNfs, **b**) SOD@$Co_3(PO_4)_2{\cdot}8H_2O$ hNfs, **c**) SOD@$Zn_3(PO_4)_2{\cdot}4H_2O$·hNfs and **d** SOD@$Mn_3(PO_4)_2{\cdot}7H_2O$·hNfs

54.23°, 55.06°, 56.37°, 57.87°, 59.11°, 60.60°, 61.34°, 66.12°, 69.35°, 71.42°, 75.07°, 77.07°, 82.11° in Fig. 6(c) compared with JCPDS (01 – 076 – 0896), and for *SOD@* $Mn_3(PO_4)_2{\cdot}7H_2O$ hNfs, XRD: 7.87°, 10.34°, 12.86°, 17.33°, 22.11°, 23.16°, 26.33°, 28.12°, 29.15°, 30.06°, 31.45°, 32.19°, 33.03°, 34.37°, 35.19°, 36.02°, 38.05°, 42.11°, 43.50°, 44.17°, 50.94°, 52.77°, 53.98°, 56.93°, 60.73°, 65.57°, 69.90° in Fig. 6(d) compared with JCPDS (00 – 003 – 0020). All XRD pattern were compared with metallophosphate structures and indexed with JCPDS numbers, and the difference of each powder pattern was recorded with 2-theta degrees. Due to the small amount of SOD used in the synthesis conditions, the peaks from SOD could not be observed clearly. All these data were recorded in accordance with the proposed structure.

Model tests for catalytic properties

The catalytic reduction reaction of the nitrophenols or organic dye to related products by various catalysts, which are mostly noble metal complexes or material/composite, is being considered as a green process with different reaction conditions. However, the catalysts bearing noble metal are expensive and unsustainable. They are also used in many technological fields and applications. Moreover, scientists are required to introduce new methodologies and catalytic systems that are eco-friendly and cost-effective in the reduction reaction of organic pollutants to corresponding reduced products. Herein, we purposed or proposed the catalytic efficiencies of SOD@metalphosphates hNfs in the reduction of 2-nitrophenol (2-NP) and Rhodamine B (RhB) with BH_4^- ion as a hydrogen source in the aqueous media at ambient temperature. The absorption spectra of catalytic reactions were monitored at a regular interval of time after the reaction steps (the testing procedure). The sample spectra were recorded from the 0 s to final times in the range of 300–600 nm for 2-NP and 400–700 nm for RhB.

Firstly, the 2-nitrophenolate (2-NP) reactant (5.0×10^{-4} M) having absorption bands at $\lambda_{max}=414$ nm (-NO_2 group of 2-NP) as a yellow color of the solution relating to the 2-nitrophenolate and the color gradually vanished due to the 2-aminophenol product. The final conversions were recorded at 60 s, 180 s, and 300 s and founded as 40.4%, 92.4%, 93.5% for SOD@$Cu_3(PO_4)_2{\cdot}3H_2O$ hNfs, 22.1%, 26.6%, 32.1% SOD@$Co_3(PO_4)_2{\cdot}8H_2O$ hNfs, 15.1%, 16.2%, 18.8% for SOD@$Zn_3(PO_4)_2{\cdot}4H_2O$ hNfs and 15.2%, 16.3%, 20.1% for SOD@$Mn_3(PO_4)_2{\cdot}7H_2O$ hNfs, respectively (Fig. 7). According to the obtained data, the catalytic activity order of SOD@metal (II) (Cu(II), Co(II), Zn(II), and Mn(II)) nanoflowers is as follows; SOD@$Cu_3(PO_4)_2{\cdot}3H_2O$ hNfs > SOD@$Co_3(PO_4)_2{\cdot}8H_2O$ hNfs > SOD@

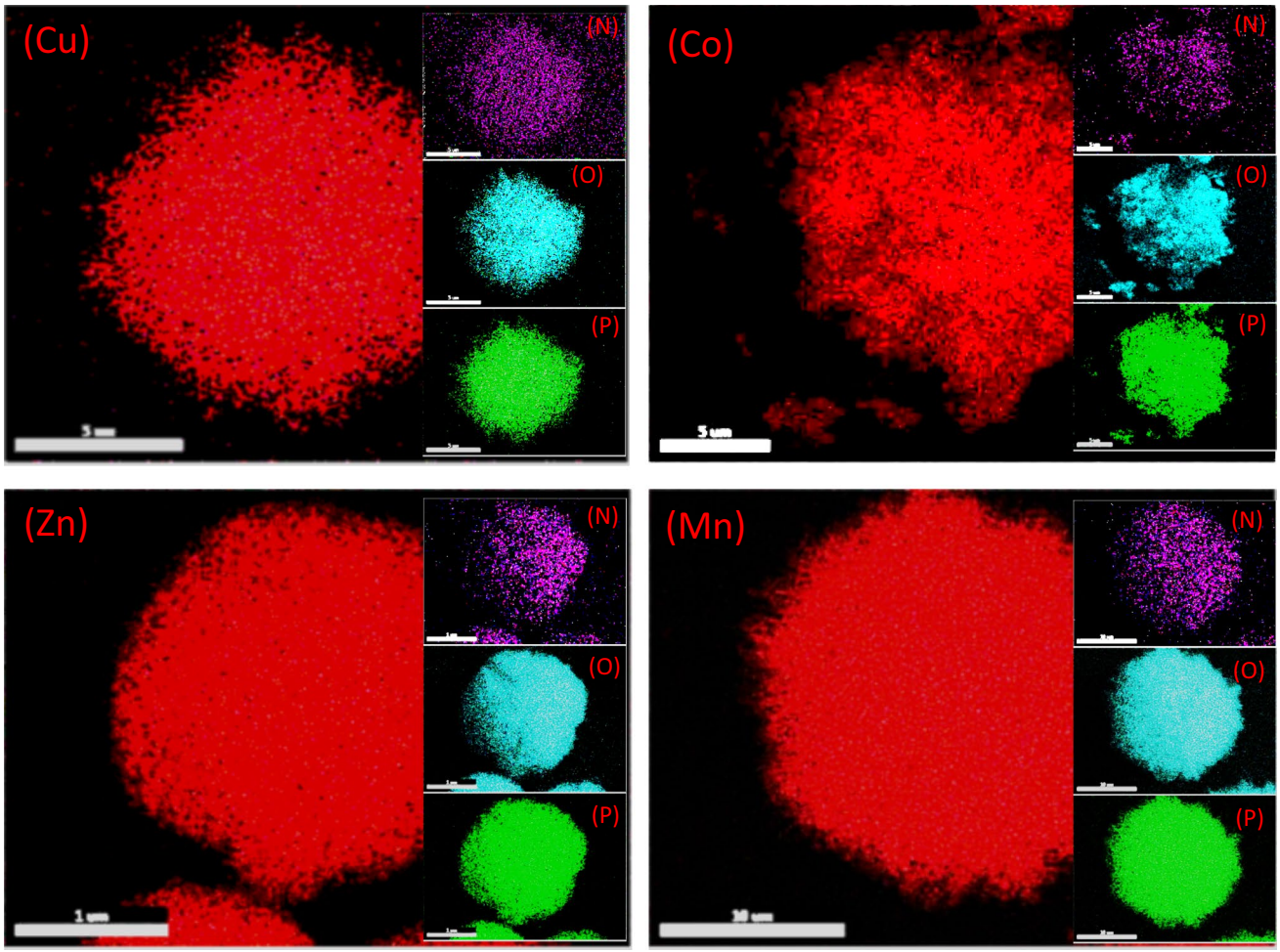

Fig. 4 Elemental mapping (N, O, P, Cu, Co, Zn, Mn) of SOD@$Cu_3(PO_4)_2{\cdot}3H_2O$ hNfs, SOD@$Co_3(PO_4)_2{\cdot}8H_2O$ hNfs, SOD@$Zn_3(PO_4)_2{\cdot}4H_2O$ hNfs, and SOD@$Mn_3(PO_4)_2{\cdot}7H_2O$·hNfs, respectively

$Mn_3(PO_4)_2{\cdot}7H_2O$ hNfs > SOD@$Zn_3(PO_4)_2{\cdot}4H_2O$ hNfs. Herein, the SOD@Cu(II) hNfs catalyst is 2.5 × superior to others (Co(II), Zn(II), and Mn(II) nanoflowers). This study is a strong indicator that catalytic activities of nanoflowers, which use the same enzyme and solutions, change dramatically with the different metals (Cu(II), Co(II), Zn(II), and Mn(II)).

Catalytic tests were also performed for Rhodamine B, which is an organic contaminant commonly used to perform a similar comparison. The main purpose here is to check if there is a change in the most active catalyst sequence when different substrates are used. It is also to clarify the effect of changes in metal centers of the fabricated nanoflowers. Figure 8 shows the Rhodamine B (RhB) reduction reaction by BH_4^- as hydrogen source while using the SOD@metalphosphates hNfs (Cu(II), Co(II), Zn(II), and Mn(II)) as effective catalysts. The aqueous solution of Rhodamine B (Rh B) demonstrated a broad and distinct peak at 550 nm in its UV–Vis spectra. All the materials (SOD@metalphosphates (Cu(II), Co(II), Zn(II), and Mn(II)) hNfs) catalyzed the Rh B reduction process by basic stirring at ambient temperature and the 550 nm peak disappearance was considered due to the reduction mechanism.

For the reduction process of Rh B, the catalytic conversions at 60 s and 900 s were achieved as 45.0%, 94.3% for SOD@$Cu_3(PO_4)_2{\cdot}3H_2O$ hNfs, 34.1%, 82.4% for SOD@$Co_3(PO_4)_2{\cdot}8H_2O$ hNfs, 32.1%, 33.2% for SOD@$Zn_3(PO_4)_2{\cdot}4H_2O$ hNfs, 29.6%, 50.1% for SOD@$Mn_3(PO_4)_2{\cdot}7H_2O$ hNfs, and 26.4%, 57.9% for SOD-free. Likewise, the catalytic efficiencies order of SOD@Metal(II) (Cu(II), Co(II), Zn(II), and Mn(II)) materials in the reduction of Rh B is as follows; SOD@$Cu_3(PO_4)_2{\cdot}3H_2O$ hNfs > SOD@$Co_3(PO_4)_2{\cdot}8H_2O$ hNfs > SOD@$Mn_3(PO_4)_2{\cdot}7H_2O$ hNfs > SOD@$Zn_3(PO_4)_2{\cdot}4H_2O$ hNfs > SOD-free.

Herein, it was noteworthy that both nitrophenol and Rhodamine B substrate had the same catalytic sequence. This explains that the metal center has a significant effect on the catalytic cycle. In our previous studies, we have

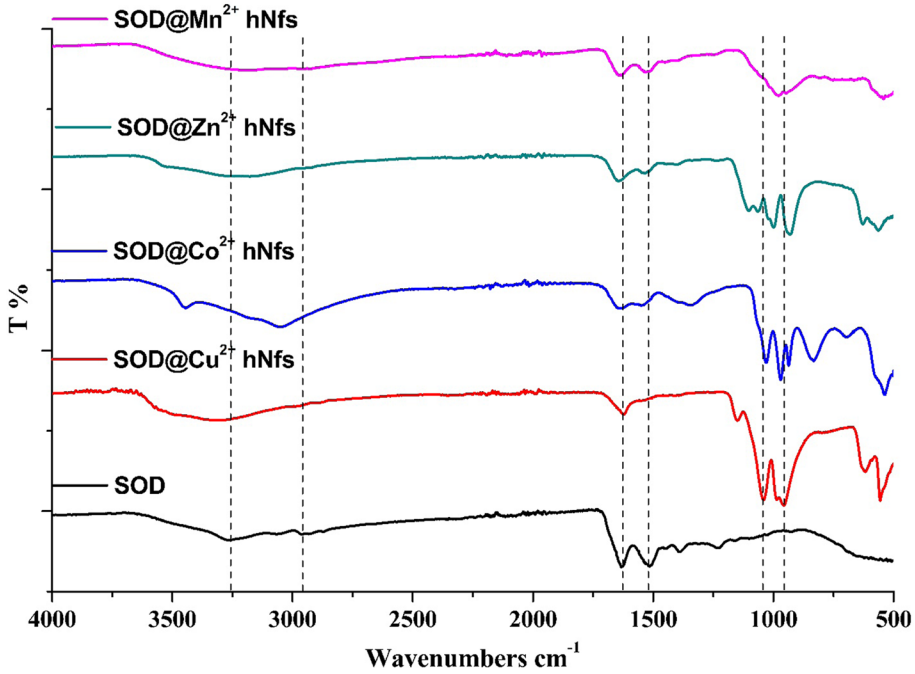

Fig. 5 FT-IR spectra of SOD, SOD@$Cu_3(PO_4)_2{\cdot}3H_2O$ hNfs, SOD@$Co_3(PO_4)_2{\cdot}8H_2O$ hNfs, SOD@$Zn_3(PO_4)_2{\cdot}4H_2O$ hNfs, and SOD@$Mn_3(PO_4)_2{\cdot}7H_2O$ hNfs

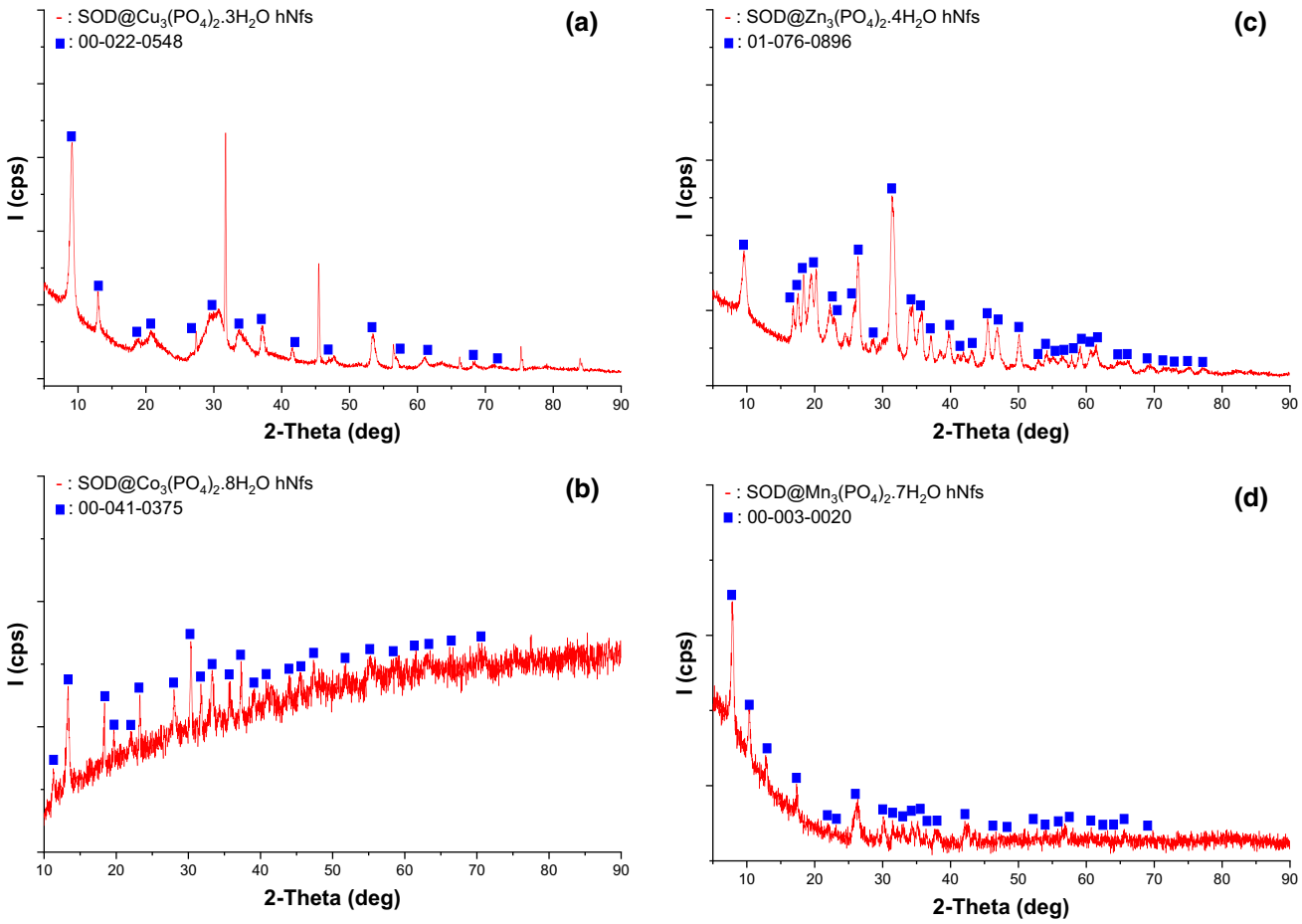

Fig. 6 X-ray diffraction analysis of **a** SOD@$Cu_3(PO_4)_2{\cdot}3H_2O$ hNfs **b** SOD@$Co_3(PO_4)_2{\cdot}8H_2O$ hNfs, **c** SOD@$Zn_3(PO_4)_2{\cdot}4H_2O$ hNfs and **d** SOD@$Mn_3(PO_4)_2{\cdot}7H_2O$ hNfs

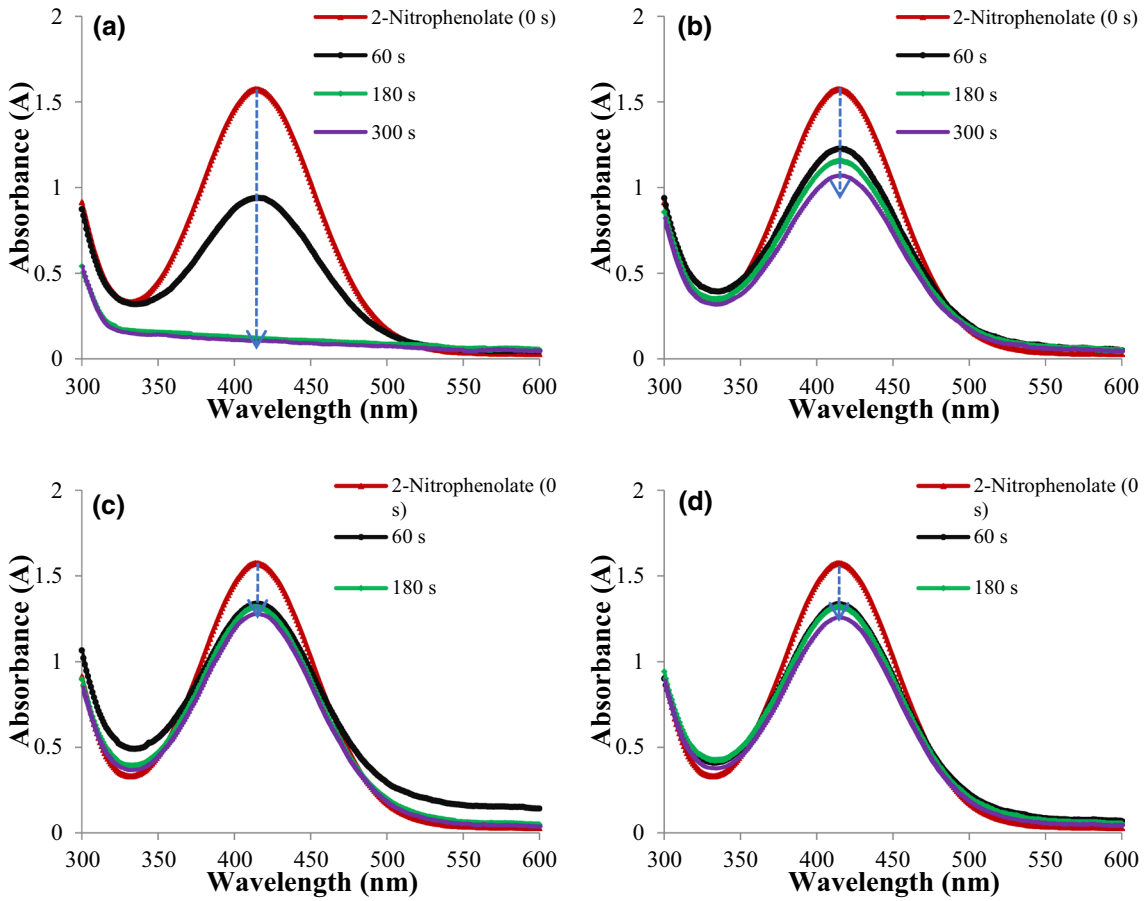

Fig. 7 Time-dependent UV–vis absorption spectra of the 2-nitrophenol (5.0×10^{-4} M) reduced by $NaBH_4$ catalyzed by the SOD@metalphosphates hNfs (Cu(II), Co(II), Zn(II), and Mn(II)), respectively

partially demonstrated an increase in performance due to the difference in the metal center (Dayan, Altinkaynak, et al. 2020). In this study, we have seen that when we compare four different metals, their tendency in the reduction reaction is the same even if the substrate changes. However, different catalytic trends can be observed by performing experiments on different substrates. Kinetic parameters were calculated to analyze the results in detail and compare them with the literature.

To determine the kinetic equation for the reduction of organic pollutants, the λ_{max} (nm) values were created due to the corresponding equation; $\ln(C_t/C_0) = -kt$, where t is time for the catalytic reaction and, k is the apparent first-order rate constant (s^{-1}) in Table 1. In the kinetic equation, C_0 and C_t values were calculated the absorbance values were noted by spectrophotometrically at the desired time (t) and k. Also, the k' = k/M parameters (M: the amount of the catalyst) were calculated for quantitative comparison and the values were determined as the ratio of the rate constant k to the weight of the catalyst added (Kamal 2019; Liang et al. 2018; Ahsan et al. 2019). All the parameters of SOD@metalphosphates (Cu(II), Co(II), Zn(II) and Mn(II)) hNfs are compared in Table 1.

Considering the kinetic parameters, it is clear that the material SOD@$Cu_3(PO_4)_2{\cdot}3H_2O$ hNfs was found as an effective catalyst in the reduction of both 2-nitrophenol and Rhodamine B substrate. This performance is demonstrated by kinetic plots of ln (C_t/C_0) vs. reaction time in Fig. 9.

Catalytic efficiency or activity depends both on the catalyst and on the substrates, media, reaction conditions (Hatamifard et al. 2016; Zhang et al. 2019; Li et al. 2020; Mwansa and Page 2020). The system is designed according to many parameters such as a surface area for materials, difference of functional groups, particle size, solubility, stability, surface morphology and redox potentials of metal ions (Goyal et al. 2014; Khodadadi et al. 2017; Hatamifard et al. 2015; Sajjadi, Nasrollahzadeh, and Tahsili 2019; Mateen et al. 2019; Guo et al. 2020; Zhu et al. 2020). The nanocomposite/materials containing metal ions have been recorded many times as effective catalysts in the reduction reactions of nitro compounds (Liu et al. 2018; Cui et al. 2018; Begum et al. 2016; Huang

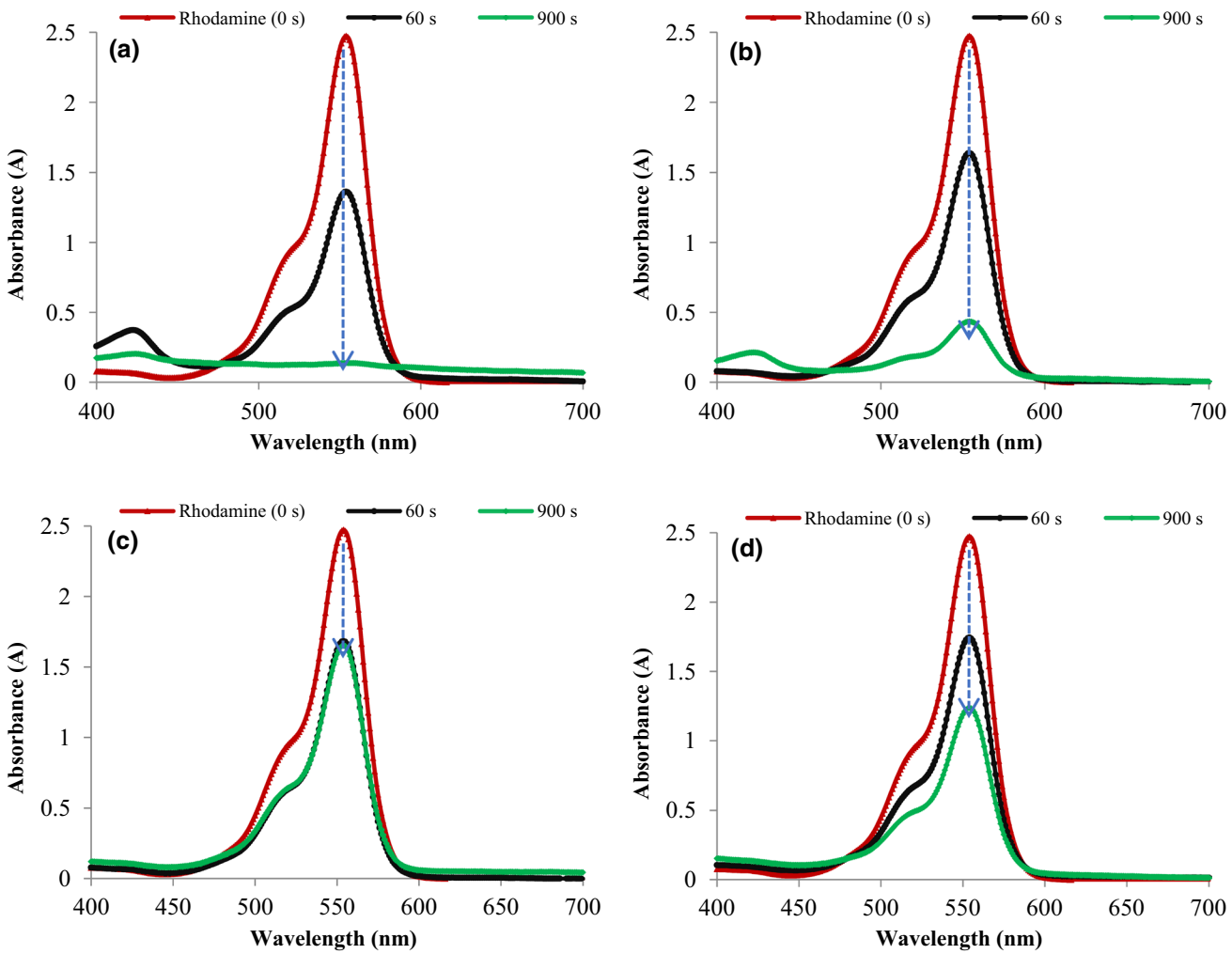

Fig. 8 Time-dependent UV–Vis absorption spectra of the Rhodamine B (10 ppm) reduced by $NaBH_4$ catalyzed by the SOD@metalphosphates hNfs (Cu(II), Co(II), Zn(II), and Mn(II)), respectively

Table 1 The catalytic efficiency rate constant of SOD@metalphosphates (Cu(II), Co(II), Zn(II), and Mn(II)) hNfs

Catalyst	Substrate	k (s^{-1})[a]			k/M (s^{-1} g^{-1})[b]		
SOD@$Cu_3(PO_4)_2$ $3H_2O$ hNfs	2-NP	8.62E-03[c]	1.43E-02[d]	9.09E-03[e]	8.62E+00[c]	1.43E+01[d]	9.09E+00[e]
SOD@$Co_3(PO_4)_2$ $8H_2O$ hNfs	2-NP	4.17E-03[c]	1.72E-03[d]	1.29E-03[e]	4.17E+00[c]	1.72E+00[d]	1.29E+00[e]
SOD@$Zn_3(PO_4)_2$ $4H_2O$ hNfs	2-NP	2.72E-03[c]	9.83E-04[d]	6.95E-04[e]	2.72E+00[c]	9.83E-01[d]	6.95E-01[e]
SOD@$Mn_3(PO_4)_2$ $7H_2O$ hNfs	2-NP	2.75E-03[c]	9.87E-04[d]	7.48E-04[e]	2.75E+00[c]	9.87E-01[d]	7.48E-01[e]
SOD@$Cu_3(PO_4)_2$ $3H_2O$ hNfs	Rh B	9.97E-03[c]	3.19E-03[f]	9.97E+00[c]	3.19E+00[f]		
SOD@$Co_3(PO_4)_2$ $8H_2O$ hNfs	Rh B	6.94E-03[c]	1.93E-03[f]	6.94E+00[c]	1.93E+00[f]		
SOD@$Zn_3(PO_4)_2$ $4H_2O$ hNfs	Rh B	6.44E-03[c]	4.49E-04[f]	6.44E+00[c]	4.49E-01[f]		
SOD@$Mn_3(PO_4)_2$ $7H_2O$ hNfs	Rh B	5.84E-03[c]	7.72E-04[f]	5.84E+00[c]	7.72E-01[f]		

[a]The reaction rate constant. [b]The reaction rate constant per total weight of tested catalyst (1 mg). [c] 60 s, [d] 180 s, [e] 300 s, [f] 900 s

et al. 2018; Shokouhimehr 2015; Nasrollahzadeh et al. 2018; Dileepkumar et al. 2020; Attatsi and Nsiah 2020; Tijani et al. 2019; Mei et al. 2019; Azadbakht et al. 2020; Shao and Sadeghzadeh 2021). Many alternative reaction mechanisms for the reduction of nitro compounds have also been proposed by scientists (Mahata et al. 2008; El-Hout et al. 2015; de Loera et al. 2018; Liu et al. 2020).

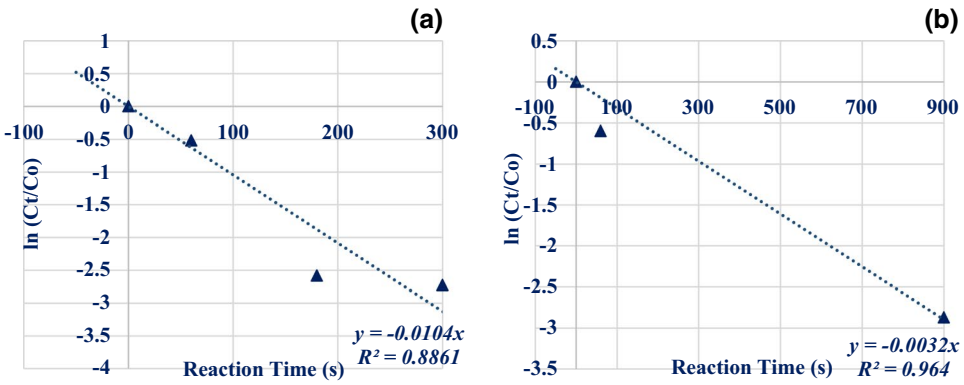

Fig. 9 Time-dependent kinetic plots of ln (C_t/C_0) for the degradation of 2-nitrophenol **a** and Rhodamine B **b** with SOD@$Cu_3(PO_4)_2{\cdot}3H_2O$ hNfs material

The catalytic mechanism for the reduction of organic pollutants with $NaBH_4$ in water has been extensively documented in earlier reports (Kamal et al. 2017, 2016). For these catalytic cycles, it is stated that the substrate (anion or cation) and the BH_4^- ions adsorb on the catalytic material surface for heterogeneous catalysts. Herein, the metal ions (Cu(II), Co(II), Zn(II), and Mn(II)) onto the SOD enzyme and phosphate ligand played a catalytic center. The metal ions (Cu(II), Co(II), Zn(II), and Mn(II)) simply facilitate the electron transfer from the adsorbed BH_4^- ions to the corresponding substrate. We observed the effect of different metals on catalytic activity and revealed this difference with their results. We anticipate that the catalytic activity of such nanoflowers can be increased with different modifications. It is also known that the SOD molecule is reduced by $NaBH_4$ (Viglino et al. 1985). It may also be possible for many macromolecules or ligands, such as the SOD. Herein, the SOD molecule is isolated as a stable nanomaterial in the form of hybrid material before being added to the same medium as $NaBH_4$. At the same time, the concentrations of both the SOD molecule and $NaBH_4$ are low in the catalytic system. For this reason, it is thought that it will not affect the performance of the catalyst to a large extent.

For catalytic efficiency of the synthesized SOD@$Cu_3(PO_4)_2{\cdot}3H_2O$ hNfs hybrid materials, a reusability (recycling) study for 2-nitrophenol (2-NP) at 300 s were performed as 5 × in the optimized (same) reaction conditions (In each reaction, the catalysts were centrifuged and washed with deionized water (3 × 2 ml).) (% Conversion = ([A_0–At]/A_0) × 100, A0 is the absorbance at time ($t = 0$) (Fig. 10). The recycles (I–V) were recorded as 93.5%, 85.1%, 74.5%, 69.7%, 61.7% (the performance loss was achieved in the last 2 cycles). With respect to the reusability study, the conversions were found to be good-moderate results and if developed, it may be suitable for economic purposes as well. The FT-IR spectrum after the recycling work of SOD@$Cu_3(PO_4)_2{\cdot}3H_2O$ hNfs hybrid materials are given in Figure S1. The metallophosphate structures are generally known to be insoluble in aqueous media. Some differences in these solubility levels may also occur due to the ligand effect.

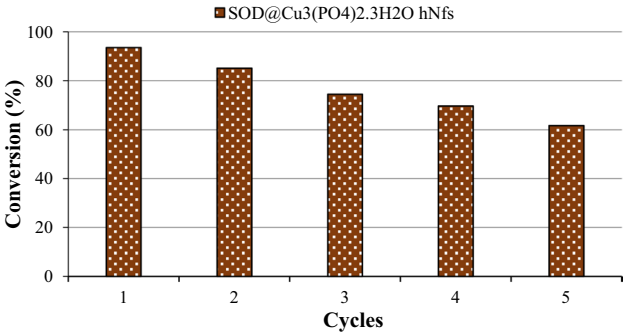

Fig. 10 The reusability studies of SOD@$Cu_3(PO_4)_2{\cdot}3H_2O$ hNfs as a catalyst for the degradation of 2-nitrophenol (2-NP) at 300 s (SOD, superoxide dismutase)

However, it was recorded that the catalyst showed moderate performance and stability in aqueous media.

In our previous studies, it was determined that the nanoflowers used for this purpose retained their chemical structures despite losing their morphological structures (Alhayali et al. 2021; Dayan, Altinkaynak, et al. 2020). Likewise, it was noted that the chemical structure of the hybrid material was preserved here as well.

The use of hybrid nanoflowers with $NaBH_4$ in reduction reactions was carried out for the first time by our research group (Dayan, Altinkaynak, et al. 2020) and, the catalytic substrates such as 2-nitroaniline, 4-nitroaniline, nitrobenzene were used in our studies (Dayan, Altinkaynak, et al. 2020; Alhayali et al. 2021). In this work, both 2-nitrophenol as another nitroarene group, and Rhodamine B as an organic pollutant, were tested in the degradation reactions. We developed and diversified our catalyst design with the experience we gained from our previous work. We have already seen that the metal center actively plays a role in catalytic activity.

Similarly, herein, it was noted that Cu, Co, Zn, and Mn metal ions had different catalytic activities. It was also found that the SOD enzyme, as an organic group, had an activity alone. When the data in here were evaluated, both a decrease in reaction times and a significant increase in conversion

Table 2 The comparative data for hybrid nanoflowers in the reduction reactions

Catalyst	Substrate	Time (s)	Conversion %	References
SOD@$Cu_3(PO_4)_2$ 3H_2O hNfs	2-Nitrophenol	300	93.50	Present study
SOD@$Co_3(PO_4)_2$ 8H_2O hNfs	2-Nitrophenol	300	32.10	Present study
SOD@$Zn_3(PO_4)_2$ 4H_2O hNfs	2-Nitrophenol	300	18.80	Present study
SOD@$Mn_3(PO_4)_2$ 7H_2O hNfs	2-Nitrophenol	300	20.10	Present study
Catalase/Fe_3O_4@Cu^{2+} hNFs at pH 7.4	2-Nitroaniline	1800	72.52	(Alhayali et al. 2021)
Catalase/Fe_3O_4@Cu^{2+} hNFs at pH 7.4	4-Nitroaniline	1800	68.60	(Alhayali et al. 2021)
Catalase/Fe_3O_4@Cu^{2+} hNFs·at pH 7.4	Nitrobenzene	1800	49.60	(Alhayali et al. 2021)
TPP@CuhNfs	2-Nitroaniline	720	94.00	(Dayan, Altinkaynak, et al. 2020)
TPP@CuhNfs	4-Nitroaniline	720	98.00	(Dayan, Altinkaynak, et al. 2020)
TPP@CuhNfs	Nitrobenzene	720	90.00	(Dayan, Altinkaynak, et al. 2020)
TPP@CohNfs	2-Nitroaniline	720	64.00	(Dayan, Altinkaynak, et al. 2020)
TPP@CohNfs	4-Nitroaniline	720	98.00	(Dayan, Altinkaynak, et al. 2020)
TPP@CohNfs	Nitrobenzene	720	91.00	(Dayan, Altinkaynak, et al. 2020)
SOD@$Cu_3(PO_4)_2$·3H_2O hNfs	Rhodamine B	900	94.30	Present study
SOD@$Co_3(PO_4)_2$·8H_2O hNfs	Rhodamine B	900	82.40	Present study
SOD@$Zn_3(PO_4)_2$·4H_2O hNfs	Rhodamine B	900	33.20	Present study
SOD@$Mn_3(PO_4)_2$·7H_2O hNfs	Rhodamine B	900	50.10	Present study

percentage were noted in terms of catalytic performance. Compared to Catalase/Fe_3O_4@Cu^{2+} hNFs at pH 7.4, TPP@CuhNfs, and TPP@CohNfs catalysts that we have produced previously, the performance of our most active catalyst (SOD@$Cu_3(PO_4)_2$.3H_2O hNfs) in this work is a quite good catalyst (Table 2). Thus, the production of a higher performance catalyst has been made possible compared to its counterparts in the literature.

Conclusion

To summarize, we have fabricated an eco-friendly approach to forming the phenomena named organic–inorganic hybrid nanoflower from superoxide dismutase (SOD), phosphate-buffered saline (PBS), Cu(II), Co(II), Zn(II), and Mn(II) salts as starting materials. The characterization analyses of the fabricated SOD@metalphosphates (Cu(II), Co(II), Zn(II), and Mn(II)) hNfs were performed by FESEM, EDX, XRD, FT-IR methods and the results confirm that the SOD macromolecule assembled on the Metal(II) hNfs. Also, we tested all the fabricated SOD@ SOD@metalphosphates (Cu(II), Co(II), Zn(II), and Mn(II)) hNfs as a catalyst in the one-pot reduction reaction of 2-nitrophenol and Rhodamine B in the water at ambient temperature. Herein, the catalytic efficiency of the SOD@metalphosphates (Cu(II), Co(II), Zn(II), and Mn(II)) hNfs has been recorded to be regarding the metal ion center types of the fabricated nanoflowers. The catalytic activity ranking for both substrates was found as SOD@$Cu_3(PO_4)_2$·3H_2O hNfs > SOD@$Co_3(PO_4)_2$·8H_2O hNfs > SOD@$Mn_3(PO_4)_2$·7H_2O hNfs > SOD@$Zn_3(PO_4)_2$·4H_2O hNfs. The facile and ecological approach to fabricating nanoflowers demonstrates that these materials can have high catalytic activity in short-time and water at ambient temperature.

Supplementary Information The online version contains supplementary material available at https://doi.org/10.1007/s11696-022-02179-z.

Acknowledgements This study was supported by Erciyes University Scientific Research Projects Unit with the project coded FDK-2016-6637 and was conducted at the Department of Chemistry, Erciyes University.

Data availability The data that support the findings of this study are available from the corresponding author upon reasonable request.

Declarations

Conflict of interest The authors declare no financial interest.

References

Advani JH, Ravi K, Naikwadi DR, Bajaj HC, Gawande MB, Biradar AV (2020) Bio-waste chitosan-derived N-doped CNT-supported Ni nanoparticles for selective hydrogenation of nitroarenes. Dalton Trans 49:10431–10440

Ahmadpoor F, Nasrollahzadeh M, Mohammad M (2021) Self-assembled lignosulfonate-inorganic hybrid nanoflowers and their application in catalytic reduction of methylene blue and 4-nitrophenol. Sep Purif Technol 272:118864

Ahsan MA, Jabbari V, El-Gendy AA, Curry ML, Noveron JC (2019) Ultrafast catalytic reduction of environmental pollutants in water via MOF-derived magnetic Ni and Cu nanoparticles encapsulated in porous carbon. Appl Surf Sci 497:143608

Alhayali NI, Ozpozan NK, Dayan S, Ozdemir N, Yilmaz BS (2021) Catalase/Fe_3O_4@Cu_2+ hybrid biocatalytic nanoflowers fabrication and efficiency in the reduction of organic pollutants. Polyhedron 194:114888

Altinkaynak C, Yilmaz I, Koksal Z, Ozdemir H, Ocsoy I, Ozdemir N (2016) Preparation of lactoperoxidase incorporated hybrid nanoflower and its excellent activity and stability. Int J Biol Macromol 84:402–409

Altinkaynak C, Gulmez C, Atakisi O, Ozdemir N (2020) Evaluation of organic-inorganic hybrid nanoflower's enzymatic activity in the presence of different metal ions and organic solvents. Int J Biol Macromol 164:162–171

Ansari S, Khorshidi A, Shariati S (2019) Synthesis of ultrafine silver nanoparticles on the surface of Fe_3O_4@SiO2@KIT-6-NH2 nanocomposite and their application as a highly efficient and reusable catalyst for reduction of nitrofurazone and aromatic nitro compounds under mild conditions. Catal Lett 149:410–418

Arsalan A, Alam MF, Zofair SFF, Ahmad S, Younus H (2020) Immobilization of beta-galactosidase on tannic acid stabilized silver nanoparticles: a safer way towards its industrial application. Spectrochim Acta Part A-Mol Biomol Spectrosc 226:117637

Attatsi IK, Nsiah F (2020) Application of silver nanoparticles toward Co(II) and Pb(II) ions contaminant removal in groundwater. Appl Water Sci 10(6):1–13

Aydemir D, Gecili F, Ozdemir N, Ulusu NN (2020) Synthesis and characterization of a triple enzyme-inorganic hybrid nanoflower (TrpE@ihNF) as a combination of three pancreatic digestive enzymes amylase, protease and lipase. J Biosci Bioeng 129:679–686

Azadbakht R, Menati S, Rudbari HA, Keypour MM (2020) Deposited silver nanoparticles on commercial copper by galvanic displacement as an effective catalyst for the reduction of 4-nitrophenol in aqueous solution. Catal Lett 150:3214–3222

Bahadorikhalili S, Arshadi H, Afrouzandeh Z, Ma'mani L (2020) Ultrasonic promoted synthesis of Ag nanoparticle decorated thiourea-functionalized magnetic hydroxyapatite: a robust inorganic-organic hybrid nanocatalyst for oxidation and reduction reactions. New J Chem 44:8840–8848

Begum R, Naseem K, Ahmed E, Sharif A, Farooqi ZH (2016) Simultaneous catalytic reduction of nitroarenes using silver nanoparticles fabricated in poly(N-isopropylacrylamide-acrylic acid-acrylamide) microgels. Coll Surf A-Physchem Eng Asp 511:17–26

Cui XL, Zhou X, Dong ZP (2018) Ultrathin gamma-Fe_2O_3 nanosheets as a highly efficient catalyst for the chemoselective hydrogenation of nitroaromatic compounds. Catal Commun 107:57–61

Das P, Ghosh S, Baskey M (2019) Heterogeneous catalytic reduction of 4-nitroaniline by RGO-Ni nanocomposite for water resource management. J Mater Sci-Mater Electron 30:19731–19737

Dayan S, Arslan F, Ozpozan NK (2015a) Ru(II) impregnated Al_2O_3, Fe_3O_4, SiO_2 and N-coordinate ruthenium(II) arene complexes: multifunctional catalysts in the hydrogenation of nitroarenes and the transfer hydrogenation of aryl ketones. Appl Catal B-Environ 164:305–315

Dayan S, Ozturk S, Kayaci N, Ozpozan NK, Ozturk E (2015b) Fabrication of MgAl2Si2O8: M-0.01 (M = Ni2+, Cu2+, Pd2+, Pt2+ and Ru3+): catalytic effects for the reduction of 2-or 4-nitroanilines in water. Bull Mater Sci 38:1651–1663

Dayan S, Altinkaynak C, Kayaci N, Dogan SD, Ozdemir N, Ozpozan NK (2020a) Hybrid nanoflowers bearing tetraphenylporphyrin assembled on copper(II) or cobalt(II) inorganic material: a green efficient catalyst for hydrogenation of nitrobenzenes in water. Appl Organomet Chem 34(3):5381

Dayan S, Kayaci N, Dayan O, Ozdemir N, Ozpozan NK (2020b) Nickel (II) complex [NiCl2(DMF)(2)L-2] bearing diaminobenzene and sulfonamide: crystal structure and catalytic application in the reduction of nitrobenzenes. Polyhedron 175:114181

Dayan S, Kayaci N, Ozdemir N, Dayan O, Ozpozan NK (2020c) Palladium(II) complexes assembled on solid materials: as catalysts for the -NO_2 (nitro) to -NH_2 (amine) reactions. Monatshefte Fur Chemie 151:1533–1548

de Loera D, Leyva E, Moctezuma E (2018) Mechanistic studies on the photocatalytic reduction of nitroaromatic compounds. Curr Org Chem 22:1475–1485

Dell'Anna MM, Intini S, Romanazzi G, Rizzuti A, Leonelli C, Piccinni F, Mastrorilli P (2014) Polymer supported palladium nanocrystals as efficient and recyclable catalyst for the reduction of nitroarenes to anilines under mild conditions in water. J Molecul Catal A-Chem 395:307–314

Denizalti S, Dayan S, Gunnaz S, Sahin E (2020) Thiazoline-Iridium (III) complexes and ımmobilized nanomaterials as selective catalysts in N-alkylation of amines with alcohols. Appl Organomet Chem 34(12):5970

Dileepkumar VG, Surya PS, Pratapkumar C, Viswanatha R, Ravikumar CR, Kumar MRA, Muralidhara HB, Al-Akraa IM, Mohammad AM, Chen Z, Bui XT, Santosh MS (2020) $NaFeS_2$ as a new photocatalytic material for the degradation of industrial dyes. J Environ Chem Eng 8(4):104005

Du JT, Shi J, Sun Q, Wang D, Wu H, Wang JX, Chen JF (2020) High-gravity-assisted preparation of aqueous dispersions of monodisperse palladium nanocrystals as pseudohomogeneous catalyst for highly efficient nitrobenzene reduction. Chem Eng J 382:122883

Durak I, Canbolat O, Kavutcu M, Ozturk HS, Yurtarslani Z (1996) Activities of total, cytoplasmic and mitochondrial superoxide dismutase enzymes in sera and pleural fluids from patients with lung cancer. J Clin Lab Anal 10:17–20

El-Hout SI, El-Sheikh SM, Hassan HMA, Harraz FA, Ibrahim IA, El-Sharkawy EA (2015) A green chemical route for synthesis of graphene supported palladium nanoparticles: a highly active and recyclable catalyst for reduction of nitrobenzene. Appl Catal A-Gen 503:176–185

Erdem HU, Kalin R, Ozdemir N, Ozdemir H (2015) Purification and biochemical characterization of peroxidase isolated from white cabbage (Brassica Oleracea var. capitata f. alba). Int J Food Prop 18:2099–2109

Fu MH, Xing JF, Ge ZQ (2019) Preparation of laccase-loaded magnetic nanoflowers and their recycling for efficient degradation of bisphenol A. Sci Total Environ 651:2857–2865

Gao JJ, Liu H, Tong C, Pang LY, Feng YQ, Zuo MG, Wei ZQ, Li JQ (2020) Hemoglobin-Mn-3(PO4)(2) hybrid nanoflower with opulent electroactive centers for high-performance hydrogen peroxide electrochemical biosensor. Sens Actuators B-Chem 307:127628

Ge J, Lei JD, Zare RN (2012) Protein-inorganic hybrid nanoflowers. Nat Nanotechnol 7:428–432

Goyal A, Bansal S, Singhal S (2014) Facile reduction of nitrophenols: comparative catalytic efficiency of MFe2O4 (M = Ni, Cu, Zn) nano ferrites. Int J Hydrogen Energy 39:4895–4908

Guo XM, Qian C, Wan XH, Zhang W, Zhu HW, Zhang JH, Yang HX, Lin SL, Kong QH, Fan TX (2020) Facile in situ fabrication of biomorphic Co2P-Co3O4/rGO/C as an efficient electrocatalyst for the oxygen reduction reaction. Nanoscale 12:4374–4382

Hatamifard A, Nasrollahzadeh M, Lipkowski J (2015) Green synthesis of a natrolite zeolite/palladium nanocomposite and its application as a reusable catalyst for the reduction of organic dyes in a very short time. RSC Adv 5:91372–91381

Hatamifard A, Nasrollahzadeh M, Sajadi SM (2016) Biosynthesis, characterization and catalytic activity of an Ag/zeolite nanocomposite for base- and ligand-free oxidative hydroxylation of phenylboronic acid and reduction of a variety of dyes at room temperature. New J Chem 40:2501–2513

He XH, Chen L, He Q, Xiao HJ, Zhou XT, Ji HB (2017) Cytochrome P450 enzyme-copper phosphate hybrid nano-flowers with

superior catalytic performances for selective oxidation of sulfides. Chin J Chem 35:693–698
Huang HG, Tang MW, Wang XG, Zhang M, Guo SQ, Zou XJ, Lu XG (2018) Synthesis of mesoporous gamma-alumina -supported co-based catalysts and their catalytic performance for chemoselective reduction of nitroarenes. ACS Appl Mater Interface 10:5413–5428
Jia WG, Wang ZB, Zhi XT (2020) Half-sandwich ruthenium complexes with Schiff base ligands bearing a hydroxyl group: preparation, characterization and catalytic activities. Appl Organomet Chem 34(1):5289
Kamal T (2019) Aminophenols formation from nitrophenols using agar biopolymer hydrogel supported CuO nanoparticles catalyst. Polym Test 77:105896
Kamal T, Khan SB, Asiri AM (2016) Nickel nanoparticles-chitosan composite coated cellulose filter paper: an efficient and easily recoverable dip-catalyst for pollutants degradation. Environ Pollut 218:625–633
Kamal T, Ahmad I, Khan SB, Asiri AM (2017) Synthesis and catalytic properties of silver nanoparticles supported on porous cellulose acetate sheets and wet-spun fibers. Carbohyd Polym 157:294–302
Khodadadi B, Bordbar M, Nasrollahzadeh M (2017) Green synthesis of Pd nanoparticles at Apricot kernel shell substrate using Salvia hydrangea extract: catalytic activity for reduction of organic dyes. J Colloid Interface Sci 490:1–10
Kim J, Grate JW, Wang P (2006) Nanostructures for enzyme stabilization. Chem Eng Sci 61:1017–1026
Kim KH, Jeong JM, Lee SJ, Choi BG, Lee KG (2016) Protein-directed assembly of cobalt phosphate hybrid nanoflowers. J Colloid Interface Sci 484:44–50
Lee HR, Chung M, Kim MI, Ha SH (2017) Preparation of glutaraldehyde-treated lipase-inorganic hybrid nanoflowers and their catalytic performance as immobilized enzymes. Enzyme Microb Technol 105:24–29
Li HY, Yang L, Wang ZX, Jin P, Zhao JX, Chen ZF (2020) N-heterocyclic carbene as a promising metal-free electrocatalyst with high efficiency for nitrogen reduction to ammonia. J Energy Chem 46:78–86
Liang LW, Fei X, Li Y, Tian J, Xu LQ, Wang XY, Wang Y (2015) Hierarchical assembly of enzyme-inorganic composite materials with extremely high enzyme activity. RSC Adv 5:96997–97002
Liang X, Chen XW, Xiang ZL, Yan R, Xi H, Bian T, Zhang JJ, Zhao JX, Cai QH, Wang HX (2018) Design and synthesis of surface-controlled CuOx/rGO nanocomposites with unusually high efficiency in catalytic conversion of organic reactants in the presence of NaBH4. Appl Surf Sci 459:716–722
Liew KH, Rocha M, Pereira C, Pires AL, Pereira AM, Yarmo MA, Juan JC, Yusop RM, Peixoto AF, Freire C (2017) Highly active ruthenium supported on magnetically recyclable chitosan-based nanocatalyst for nitroarenes reduction. Chem CatChem 9:3930–3941
Lin Z, Xiao Y, Wang L, Yin YQ, Zheng JN, Yang HH, Chen GN (2014a) Facile synthesis of enzyme-inorganic hybrid nanoflowers and their application as an immobilized trypsin reactor for highly efficient protein digestion. RSC Adv 4:13888–13891
Lin Z, Xiao Y, Yin YQ, Hu WL, Liu W, Yang HH (2014b) Facile synthesis of enzyme-inorganic hybrid nanoflowers and its application as a colorimetric platform for visual detection of hydrogen peroxide and phenol. ACS Appl Mater Interface 6:10775–10782
Liu ZY, Wang XG, Zou XJ, Lu XG (2018) Molybdenum carbide catalysts for chemoselective transfer hydrogenation of nitroarenes. Chem Sel 3:5165–5168
Liu Q, Tadrent S, Proust C, Gomez F, Khelfa A, Luart D, Len C (2020) Theoretical analysis of the "green" synthesis of aniline by reduction of nitrobenzene. Chem Eng Sci 211:115275
Madhu A, Chakraborty JN (2017) Developments in application of enzymes for textile processing. J Clean Prod 145:114–133
Mahata N, Cunha AF, Orfao JJM, Figueiredo JL (2008) Hydrogenation of nitrobenzene over nickel nanoparticles stabilized by filamentous carbon. Appl Catal A-Gen 351:204–209
Mateen M, Shah K, Chen Z, Chen C, Li YD (2019) Selective hydrogenation of N-heterocyclic compounds over rhodium-copper bimetallic nanocrystals under ambient conditions. Nano Res 12:1631–1634
Mei H, Wang XD, Zeng T, Huang L, Wang Q, Ru DP, Huang TL, Tian FL, Wu HM, Gao JM (2019) A nanocomposite consisting of gold nanobipyramids and multiwalled carbon nanotubes for amperometric nonenzymatic sensing of glucose and hydrogen peroxide. Microchim Acta 186(4):1–8
Mohamed SA, Al-Malki AL, Kumosani TA, El-Shishtawy RM (2013) Horseradish peroxidase and chitosan: activation, immobilization and comparative results. Int J Biol Macromol 60:295–300
Moradi M, Rastakhiz N, Ghaedi M, Zhiani R (2020) DFNS/PEI/Cu Nanocatalyst for reduction of nitro-aromatic compounds. Catal Lett 151(6):1653–1662
Mwansa JM, Page MI (2020) Catalysis, kinetics and mechanisms of organo-iridium enantioselective hydrogenation-reduction. Catal Sci Technol 10:590–612
Nadar SS, Gawas SD, Rathod VK (2016) Self-assembled organic-inorganic hybrid glucoamylase nanoflowers with enhanced activity and stability. Int J Biol Macromol 92:660–669
Nasrollahzadeh M, Sajjadi M, Maham M, Sajadi SM, Barzinjy AA (2018) Biosynthesis of the palladium/sodium borosilicate nanocomposite using Euphorbia milii extract and evaluation of its catalytic activity in the reduction of chromium(VI), nitro compounds and organic dyes. Mater Res Bull 102:24–35
Netto CGCM, Toma HE, Andrade LH (2013) Superparamagnetic nanoparticles as versatile carriers and supporting materials for enzymes. J Molecul Catal B-Enzymatic 85–86:71–92
Noma SAA, Yilmaz BS, Ulu A, Ozdemir N, Ates B (2020) Development of L-asparaginase@hybrid nanoflowers (ASNase@HNFs) reactor system with enhanced enzymatic reusability and stability. Catal Lett 151(4):1191–1201
Patel SKS, Otari SV, Kang YC, Lee JK (2017) Protein-inorganic hybrid system for efficient his-tagged enzymes immobilization and its application in L-xylulose production. RSC Adv 7:3488–3494
Sajjadi M, Nasrollahzadeh M, Tahsili MR (2019) Catalytic and antimicrobial activities of magnetic nanoparticles supported N-heterocyclic palladium(II) complex: a magnetically recyclable catalyst for the treatment of environmental contaminants in aqueous media. Sep Purif Technol 227:115617
Sargin I, Baran T, Arslan G (2020) Environmental remediation by chitosan-carbon nanotube supported palladium nanoparticles: conversion of toxic nitroarenes into aromatic amines, degradation of dye pollutants and green synthesis of biaryls. Sep Purif Technol 247:116987
Sassolas A, Blum LJ, Leca-Bouvier BD (2012) Immobilization strategies to develop enzymatic biosensors. Biotechnol Adv 30:489–511
Shao ZY, Sadeghzadeh SM (2021) Fabrication of Nitrogen-enriched graphene oxide on the DFNS/Metal NPs as a nanocatalysts for the reduction of 4-Nitrophenol and 2-Nitroaniline. Catal Lett 151:1882–1893
Shcharbin D, Halets-Buis I, Abashkin V, Dzmitruk V, Loznikova S, Odabasi M, Acet O, Onal B, Ozdemir N, Shcharbina N, Bryszewska M (2019) Hybrid metal-organic nanoflowers and their application in biotechnology and medicine. Coll Surface B-Biointerface 182:110345
Sheng Y, Wang XG, Yue SN, Cheng GL, Zou XJ, Lu XG (2020) In situ synthesized silica-supported Co@N-Doped carbon as highly efficient and reusable catalysts for selective reduction of halogenated nitroaromatics. ChemCatChem 12:4632–4641

Shokouhimehr M (2015) Magnetically separable and sustainable nanostructured catalysts for heterogeneous reduction of nitroaromatics. Catalysts 5:534–560

Somturk B, Yilmaz I, Altinkaynak C, Karatepe A, Ozdemir N, Ocsoy I (2016) Synthesis of urease hybrid nanoflowers and their enhanced catalytic properties. Enzyme Microb Technol 86:134–142

Sun JY, Ge JC, Liu WM, Lan MH, Zhang HY, Wang PF, Wang YM, Niu ZW (2014) Multi-enzyme co-embedded organic-inorganic hybrid nanoflowers: synthesis and application as a colorimetric sensor. Nanoscale 6:255–262

Tijani JO, Momoh UO, Salau RB, Bankole MT, Abdulkareem AS, Roos WD (2019) Synthesis and characterization of Ag2O/B2O3/TiO2 ternary nanocomposites for photocatalytic mineralization of local dyeing wastewater under artificial and natural sunlight irradiation. Environ Sci Pollut Res 26:19942–19967

Viglino P, Scarpa M, Cocco D, Rigo A (1985) Preparation of reduced bovine Cu, Zn superoxide-dismutase. Biochem J 229:87–90

Wang LB, Wang YC, He R, Zhuang A, Wang XP, Zeng J, Hou JG (2013) A new nanobiocatalytic system based on allosteric effect with dramatically enhanced enzymatic performance. J Am Chem Soc 135:1272–1275

Wei YH, Klajn R, Pinchuk AO, Grzybowski BA (2008) Synthesis, shape control, and optical properties of hybrid Au/Fe_3O_4 "nanoflowers." Small 4:1635–1639

Wells A, Meyer HP (2014) Biocatalysis as a strategic green technology for the chemical industry. ChemCatChem 6:918–920

Weselake RJ, Chesney SL, Petkau A, Friesen AD (1986) Purification of human copper, zinc superoxide-dismutase by copper chelate affinity-chromatography. Anal Biochem 155:193–197

Wu ZF, Li X, Li FG, Yue H, He CY, Xie F, Wang Z (2014) Enantioselective transesterification of (R, S)-2-pentanol catalyzed by a new flower-like nanobioreactor. RSC Adv 4:33998–34002

Xu YL, Shi XF, Hua R, Zhang R, Yao YJ, Zhao B, Liu T, Zheng JZ, Lu G (2020) Remarkably catalytic activity in reduction of 4-nitrophenol and methylene blue by Fe_3O_4@COF supported noble metal nanoparticles. Appl Catal B-Environ 260:118142

Yin YQ, Xiao Y, Lin G, Xiao Q, Lin Z, Cai ZW (2015) An enzyme-inorganic hybrid nanoflower based immobilized enzyme reactor with enhanced enzymatic activity. J Mater Chem B 3:2295–2300

Zhang BL, Li PT, Zhang HP, Li XJ, Tian L, Wang H, Chen X, Ali N, Ali Z, Zhang QY (2016) Red-blood-cell-like BSA/Zn-3(PO4)(2) hybrid particles: preparation and application to adsorption of heavy metal ions. Appl Surf Sci 366:328–338

Zhang KQ, Suh JM, Choi JW, Jang HW, Shokouhimehr M, Varma RS (2019) Recent advances in the nanocatalyst-assisted NABH4 reduction of nitroaromatics in water. ACS Omega 4:483–495

Zhang QX, Mao Z, Wang KX, Phan NTS, Zhang F (2020) Microwave-assisted aqueous carbon-carbon cross-coupling reactions of aryl chlorides catalysed by reduced graphene oxide supported palladium nanoparticles. Green Chem 22:3239–3247

Zhao ZH, Lin TR, Liu WR, Hou L, Ye F, Zhao SL (2019) Colorimetric detection of blood glucose based on GOx@ZIF-8@Fe-polydopamine cascade reaction. Spectrochimica Acta Part a-Molecul Biomol Spectroscop 219:240–247

Zhu M, Yan YD, Yan Q, Yin JL, Cheng K, Ye K, Zhu K, Yan J, Cao DX, Wang GL (2020) In situ growth of Ni0.85Se on graphene as a robust electrocatalyst for hydrogen evolution reaction. Int J Hydrogen Energy 45:10486–10493